Nonlinear Filtering for a Nonlinear Vision-Based System for the Relative Tracking of Two Marine Vehicles

Sophie Chareyron and Michael Athans

Abstract— **We present a feasibility study of a nonlinear vision-based tracking system to provide estimates of the position and velocity of an Autonomous Underwater Vehicle (AUV) relative to an Autonomous Surface Craft (ASC). Non linear estimator designs are implemented using the theory of extended Kalman filtering and second order filtering. Simulations illustrate the performance of the estimators.**

Keywords— **Estimation, Nonlinear Filtering, Kalman Filter, Underwater Vehicles.**

I. Introduction

In recent years a project based on the communication between an Autonomous Underwater Vehicle (AUV) and an Autonomous Surface Craft (ASC) has been on-going [1], [2]. The aim is to study the extent of shallow water hydrothermalism and to determine the patterns of community diversity at the vents in the Azores. Sensors carried by the AUV (such as video camera and sonar) collect scientific data in a pre-specified survey area.

In order to be able to modify in real time the data stored by the AUV, a joint cooperative mission is required. Data exchange between the two vehicles must rely on acoustic communications due to the strong attenuation experienced by electromagnetic waves in the water. In order to have access to higher bandwidth acoustic communications, the vertical channel must be used. This constraint motivates to position both the AUV and the ASC at the same vertical position.

These requirements lead naturally to the need to implement a tracker on board of the ASC to provide access to estimates of the relative position and velocity of both platforms. The proposed solution in the following work relies on the use of two sensors. The first one is a calibrated video camera on the ASC. This provides the coordinates of an artificial feature of the AUV (such as a strobe light) in the image. The camera maps 3D into 2D image coordinates. An additional measurement, AUV depth is also made. The depth cell carried by the AUV will transmit its depth through the acoustic communication link.

The object of this study is the development of a vision based tracker. In [3] a similar goal was achieved using the theory of Linear Parametrically Varying (LPV) systems. We propose here an approach using the theory of extended Kalman filtering. In section II the modelling of the system dynamics is described. In section III a first simulation allows us to analyze the performance of our tracker under "normal" plant and sensor noises, and observe the estimates of relative position and relative velocity for both platforms for different initial state uncertainty. In section IV , we study the performance of the tracker under three different covariance matrices for the plant noise processes.

M. Athans is with Instituto Superior Técnico, Instituto de Sistemas e Robótica, Av. Rovisco Pais, 1049–001 Lisboa, Portugal. Email: athans@isr.ist.utl.pt

S.Chareyron is with INRIA Rhone-Alpes,Zirst - 655 avenue de l'Europe - Montbonnot - 38334 Saint Ismier Cedex - France. Email: sophie.chareyron@inrialpes.fr

This work was realized within the Instituto Superior Técnico, Instituto de Sistemas e Robótica, Av. Rovisco Pais, 1049–001 Lisboa, Portugal

II. Tracker design

A. System Presentation

A.1 Notations

In this study, we usee three reference frames:

{I} denotes an inertial frame located at mean sea level,
{S} denotes the ASC body fixed frame ,
{U} denotes the AUV body fixed frame.

We want to estimate the relative position and velocity in the inertial reference frame. The following notations will be used:

$p(t) = [x(t); y(t); z(t)]^T$ relative position in the I frame ,
$v(t) = [v_x(t); v_y(t); v_z(t)]^T$ relative velocity in the I frame.

Figure 1 shows the platforms and the references associated with them.

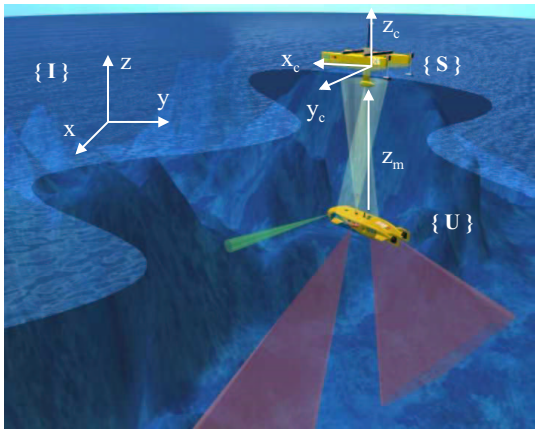

Fig. 1
The Delfim (ASC) and the Infante (AUV). Reference frames and notations.

A.2 Time varying ACS attitude

We define $\boldsymbol{\lambda}(t) = [\varphi(t); \theta(t); \psi(t)]^T$ to be the vector containing the roll, pitch and yaw angles that parameterize locally the orientation of the frame {S} with respect to {I}. The ASC is assumed to be equipped with a set of sensor and its own navigation system. At any time therefore, the values of those angles are available. Thus the rotation matrix from {S} to {I} is known at all times. It is a time varying rotation matrix, which is denoted by $\boldsymbol{R}(t)$. Since it is a rotation matrix, it satisfies the orthogonality condition: $\boldsymbol{R}^T(t)\boldsymbol{R}(t) = \boldsymbol{I}$ (or $\boldsymbol{R}^T(t) = \boldsymbol{R}^{-1}(t)$). The inverse rotation matrix $\boldsymbol{R}^{-1}(t)$ is given by

$$\boldsymbol{R}^{-1}(t) = \begin{bmatrix} \cos(\theta)\cos(\psi) & \sin(\theta)\sin(\varphi)\cos(\psi) - \cos(\varphi)\sin(\psi) & \cos(\varphi)\sin(\theta)\cos(\psi) + \sin(\varphi)\sin(\psi) \\ \sin(\psi)\cos(\theta) & \sin(\theta)\sin(\varphi)\sin(\psi) + \cos(\varphi)\cos(\psi) & \sin(\psi)\cos(\varphi)\sin(\theta) - \sin(\varphi)\cos(\psi) \\ -\sin(\theta) & \sin(\varphi)\cos(\theta) & \cos(\varphi)\cos(\theta) \end{bmatrix}, \quad (1)$$

where φ, θ and ψ are the roll, pitch and yaw angles, respectively. In order to simulate a realistic system, we will assume that the waves are a superposition of sinusoids of amplitude less than one meter and of period from five to twenty seconds. A longer period, for a wave, usually corresponds to a higher amplitude, and hence to higher roll pitch and yaw angle. In the sequel, we will use the following angle variations, as being representative of ASC attitude angles,

$$\begin{aligned} \varphi(t) &= 4\cos(\tfrac{2\pi}{5}t) + 10\cos(\tfrac{2\pi}{15}t + \tfrac{\pi}{6}), \\ \theta(t) &= 5\cos(\tfrac{2\pi}{7}t + \tfrac{\pi}{4}) + 15\cos(\tfrac{2\pi}{18}t + \tfrac{\pi}{7}), \\ \psi(t) &= 85 + 7\cos(\tfrac{2\pi}{13}t + \tfrac{\pi}{14}). \end{aligned} \quad (2)$$

A.3 Measurements

• The camera. A video camera is pointing down, and is able to discriminate some artificial feature of the AUV, such a strobe light, coincident with the origin of {U} as depicted in Figure 1. We assume that the camera has the same orientation as {S}, and is centered in {S}. Let ${}^I\boldsymbol{p}_U(t)$ and ${}^I\boldsymbol{p}_S(t)$ denote respectively the position of the AUV and of the ASC in the {I} frame. Let ${}^S\boldsymbol{p}_U(t)$ be the position of the AUV in the camera frame {S}, the relation between the position of the AUV in the {I} and {S} frames is as follows

$${}^I\boldsymbol{p}_U(t) = {}^I\boldsymbol{p}_S(t) + \boldsymbol{R}(t){}^S\boldsymbol{p}_U(t). \quad (3)$$

The coordinates $x_c(t)$, $y_c(t)$ and $z_c(t)$ of the AUV position in the camera frame ${}^S\boldsymbol{p}_U(t) = [x_c(t); y_c(t); z_c(t)]^T$ are, using (3),

$$\begin{aligned} [x_c(t); y_c(t); z_c(t)]^T &= \boldsymbol{R}^{-1}(t)({}^I\boldsymbol{p}_U(t) - {}^I\boldsymbol{p}_S(t)) \\ &= \boldsymbol{R}^{-1}(t)\boldsymbol{p}(t), \end{aligned} \quad (4)$$

with $\boldsymbol{p}(t)$ the relative position and $\boldsymbol{R}^{-1}(t)$ the inverse rotation matrix. In order to meet our requirements (camera's sensibility and worst possible error) a focal length of $f = 300mm$ is used. The camera nonlinear mapping from $\mathcal{R}^3$ to $\mathcal{R}^2$ links the 3D coordinates $x_c(t)$, $y_c(t)$ and $z_c(t)$ to the 2D coordinates $u_c(t)$ and $v_c(t)$, extracted from the image, as follows

$$\begin{bmatrix} u_c(t) \\ v_c(t) \end{bmatrix} = \begin{bmatrix} \frac{f\, x_c(t)}{z_c(t)} \\ \frac{f\, y_c(t)}{z_c(t)} \end{bmatrix}. \quad (5)$$

The key relation (5) leads to an ambiguity in the coordinate measurements in the image plane. We can solve this problem by making an additional measurement.

• The depth cell. This sensor will give us the depth of the AUV. We will assume that the wave amplitude is negligible compare to the relative depth between the two platforms. Therefore we can assume that the ASC stays at the mean sea level and that the depth cell will give us the distance (relative depth) between the two vehicles z_m, in the {I} reference. The depth, in this mission, is constant $z_m = z_c = 30m$. The magnitude of our optical system, defined as

$$M = \frac{z_c}{f} = 100, \quad (6)$$

scales the camera's measurements to the dimension of the relative position of the AUV.

In the following, the three measurement coordinates x_m, y_m and z_m are expressed as

$$[x_m; y_m; z_m] = [u_c; v_c; z_m],$$

where u_c and v_c are the 2D coordinates extracted from the image of the camera and z_m is the measurement given by the depth cell.

B. Discrete-time modelling of system dynamics

B.1 Continuous-time system dynamics

The following notations for the state (relative position and velocity), and for the measurement vectors in the inertial reference {I} are used

$$\boldsymbol{x}(t) = \begin{bmatrix} x_1(t) \\ x_2(t) \\ x_3(t) \\ x_4(t) \\ x_5(t) \\ x_6(t) \end{bmatrix} = \begin{bmatrix} x(t) \\ y(t) \\ z(t) \\ v_x(t) \\ v_y(t) \\ v_z(t) \end{bmatrix} \qquad \boldsymbol{z}(t) = \begin{bmatrix} z_1(t) \\ z_2(t) \\ z_3(t) \end{bmatrix} = \begin{bmatrix} x_m(t) \\ y_m(t) \\ z_m(t) \end{bmatrix}.$$

We assume that the speed of the AUV is constant, and that no applied forces are used. The system dynamics are as follows

$$\frac{d}{dt}\begin{bmatrix} x_1(t) \\ x_2(t) \\ x_3(t) \\ x_4(t) \\ x_5(t) \\ x_6(t) \end{bmatrix} = \begin{bmatrix} 0 & 0 & 0 & 1 & 0 & 0 \\ 0 & 0 & 0 & 0 & 1 & 0 \\ 0 & 0 & 0 & 0 & 0 & 1 \\ 0 & 0 & 0 & 0 & 0 & 0 \\ 0 & 0 & 0 & 0 & 0 & 0 \\ 0 & 0 & 0 & 0 & 0 & 0 \end{bmatrix} \begin{bmatrix} x_1(t) \\ x_2(t) \\ x_3(t) \\ x_4(t) \\ x_5(t) \\ x_6(t) \end{bmatrix} + \boldsymbol{L}\,\boldsymbol{\xi}(t). \quad (7)$$

We want to analyze the influence of the plant (acceleration) noise $\boldsymbol{\xi}(t)$, which we assume to be white noise.

B.2 Discrete-time system dynamics

The measurements are made only at discrete instant of time, every T seconds. For this reason, we will work with a discrete time version of the system. T is fixed by the

measurement of the depth cell which is sent by the AUV every second, $T = 1s$. The continuous-time dynamics (7) lead to the following discrete-time system dynamics

$$\begin{bmatrix} x_1(t+1) \\ x_2(t+1) \\ x_3(t+1) \\ x_4(t+1) \\ x_5(t+1) \\ x_6(t+1) \end{bmatrix} = \boldsymbol{A} \begin{bmatrix} x_1(t) \\ x_2(t) \\ x_3(t) \\ x_4(t) \\ x_5(t) \\ x_6(t) \end{bmatrix} + \boldsymbol{L}\, \boldsymbol{\xi}(t), \qquad (8)$$

with $\boldsymbol{A}$ and $\boldsymbol{L}$ given by

$$\boldsymbol{A} = \begin{bmatrix} 1 & 0 & 0 & 1 & 0 & 0 \\ 0 & 1 & 0 & 0 & 1 & 0 \\ 0 & 0 & 1 & 0 & 0 & 1 \\ 0 & 0 & 0 & 1 & 0 & 0 \\ 0 & 0 & 0 & 0 & 1 & 0 \\ 0 & 0 & 0 & 0 & 0 & 1 \end{bmatrix} \qquad \boldsymbol{L} = \begin{bmatrix} 0 & 0 & 0 \\ 0 & 0 & 0 \\ 0 & 0 & 0 \\ 1 & 0 & 0 \\ 0 & 1 & 0 \\ 0 & 0 & 1 \end{bmatrix}.$$

The initial time is taken to be $t = 0$. We will include in this model three discrete-time, stationary, zero-mean, plant white noises $\xi_1(t)$, $\xi_2(t)$, $\xi_3(t)$, to introduce a small stochastic variability in the plant speed. The statistics of the plant noises are assumed to be

$$\boldsymbol{\xi}(t) = [\xi_1(t); \xi_2(t); \xi_3(t)]^T,$$
$$E\{\xi_1(t)\} = 0 \qquad E\{\xi_2(t)\} = 0 \qquad E\{\xi_3(t)\} = 0.$$

Assuming that $\xi_1(t)$, $\xi_2(t)$ and $\xi_3(t)$ are uncorrelated and that each plant noise intensity is constant in time leads to the following covariance matrix of the plant noise, with constant intensity matrix $\boldsymbol{\Xi}$

$$E\{\boldsymbol{\xi}(t)\boldsymbol{\xi}^T(\tau)\} = \begin{bmatrix} 0 & 0 & 0 & 0 & 0 & 0 \\ 0 & 0 & 0 & 0 & 0 & 0 \\ 0 & 0 & 0 & 0 & 0 & 0 \\ 0 & 0 & 0 & 0.01^2 & 0 & 0 \\ 0 & 0 & 0 & 0 & 0.01^2 & 0 \\ 0 & 0 & 0 & 0 & 0 & 0.01^2 \end{bmatrix} = \boldsymbol{\Xi}\, \delta_{t\tau}.$$

This means that every second, there is an unpredictable change in each relative velocity with standard deviation $0.01m/s$.

B.3 Measurements

The measured output $\boldsymbol{z}(t)$ is composed by three measurements corrupted by additive Gaussian discrete-time white noise $\boldsymbol{\omega}(t) = [\omega_1(t); \omega_2(t); \omega_3(t)]^T$. Assuming that $\omega_1(t)$, $\omega_2(t)$ and $\omega_3(t)$ are stationary and uncorrelated, we have

$$E\{\omega_1(t)\} = 0 \qquad E\{\omega_2(t)\} = 0 \qquad E\{\omega_3(t)\} = 0$$

$$E\{\boldsymbol{\omega}(t)\boldsymbol{\omega}^T(\tau)\} = \begin{bmatrix} \Omega_1 & 0 & 0 \\ 0 & \Omega_2 & 0 \\ 0 & 0 & \Omega_3 \end{bmatrix} = \boldsymbol{\Omega}\, \delta_{t\tau}.$$

where $\boldsymbol{\Omega}$ is the constant measurement noise intensity matrix. The measurement vector, $\boldsymbol{z}(t)$, takes the form

$$\boldsymbol{z}(t) = \boldsymbol{h}(\boldsymbol{x}(t), t) + \boldsymbol{\omega}(t), \qquad (9)$$

with $\boldsymbol{h}(\boldsymbol{x}(t), t)$ being the nonlinear relation that generates the measurements from the states, which given by

$$\begin{aligned} \boldsymbol{h}(\boldsymbol{x}(t), t) &= \begin{bmatrix} h_1(\boldsymbol{x}(t), t) \\ h_2(\boldsymbol{x}(t), t) \\ h_3(\boldsymbol{x}(t), t) \end{bmatrix} \qquad (10) \\ &= \begin{bmatrix} (R^{-1}_{1,1}(t)x_1(t) + R^{-1}_{1,2}(t)x_2(t) + R^{-1}_{1,3}(t)x_3(t))\frac{f}{x_3(t)} \\ (R^{-1}_{2,1}(t)x_1(t) + R^{-1}_{2,2}(t)x_2(t) + R^{-1}_{2,3}(t)x_3(t))\frac{f}{x_3(t)} \\ x_3(t) \end{bmatrix}. \end{aligned}$$

The first two relations $h_1(\boldsymbol{x}(t), t)$ and $h_2(\boldsymbol{x}(t), t)$ are obtained from (5) i.e. the camera measurements. In (12) $R^{-1}_{i,j}(t)$ denotes the term of the i^{th} row and j^{th} column of the inverse rotation matrix $\boldsymbol{R}^{-1}(t)$, given in (1). The third equation $h_3(\boldsymbol{x}(t), t)$ is directly given by the measurement of the depth cell in the presence of white noise. The camera dynamics contain a nonlinear term $\frac{1}{x_3(t)}$. We will, therefore, need to implement nonlinear filters. In order to observe the influence of each state on the different outputs, Figure 2 shows the first row elements of the inverse rotation matrix as a function of time. Clearly, our measurements are strongly time-varying and nonlinear.

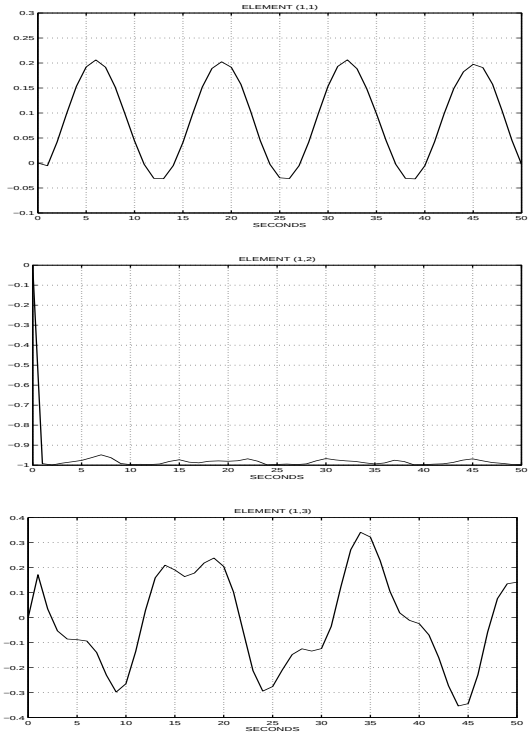

Fig. 2
$R^{-1}_{1,1}(t)$(TOP), $R^{-1}_{1,2}(t)$(MIDDLE), $R^{-1}_{1,3}(t)$ (BOTTOM)

The elements $R^{-1}_{1,1}(t)$ and $R^{-1}_{1,3}(t)$ are, in average, less than $|0.2|$ (see Figure 2 (top and bottom)), whereas the gain of $R^{-1}_{1,2}(t)$ is close to $|1|$ (see Figure 2 (middle)). Therefore the x_m coordinate reflects the y relative position according to the expression of $h_1(x, t)$ in (12) (similar figures were obtained for y_m showing that it reflects the x relative position).

Due to the average angle of 85° between inertial referential and the frame of the ASC (see (2)), $R^{-1}_{1,1}(t)$ is small compar

to $R_{1,2}^{-1}(t)$. Therefore, a relative position of $1m$ in the x (or y) direction will be represented by $1cm$ in the y_m (or x_m) output according to (6) and (12). The sensor noise intensities are fixed as follows. A standard deviation of $0.2m$ on the relative position corresponds to a standard deviation of $0.002m$ of the camera noise (see (6)). This noise intensity reflects the perturbations of under water measurements that are due to the multiple dispersion of sun light and absorption of the AUV strobe light. The additive white noise of the depth cell has a standard deviation of $0.5m$ which take into account the multiple reflection of the acoustic wave that interferes with the information. The sensor noise intensities used were as follows

$$\Omega_1 = (0.002)^2 \qquad \Omega_2 = (0.002)^2 \qquad \Omega_3 = (0.5)^2.$$

B.4 Filter design

The system is time varying due to the wave motion. This will introduce varying roll pitch and yaw angle representing the movement of our ASC. The camera, fixed to the frame of the ASC, will rely on the time varying attitude $\boldsymbol{\lambda}(t)$ of the frame of the ASC. Hence, the rotation matrix is computed at each measurement. We assume that there is no noise on the measurement of the attitude of the ASC, i.e. on $\boldsymbol{\lambda}(t)$. Due to the nonlinear term $\frac{f}{x_3}$ in (12), we need to implement a non-linear filter using the theory of the extended Kalman filtering. We can find in [4] the equations of the extended Kalman and second-order filters, and we do not repeat them here. Let $\boldsymbol{\Sigma}(t+1|t+1)$ denote the updated state covariance matrix . Because of the nonlinearity in the sensor dynamics, the updated covariance matrix is based upon continuously relinearized Jacobian matrix $\hat{\boldsymbol{C}}(t+1)$ of $\boldsymbol{h}(\boldsymbol{x}(t), t)$. Denoting the one-step predicted state estimates as $\hat{\mathrm{x}}(t+1|t)$, the $\hat{\boldsymbol{C}}(t+1)$ matrix of dimension 3×6, based upon the most recent state estimates, is given by

$$\hat{\boldsymbol{C}}(t+1) = \begin{bmatrix} R_{1,1}^{-1}\frac{f}{\hat{\mathrm{x}}_3(t+1|t)} & R_{1,2}^{-1}\frac{f}{\hat{\mathrm{x}}_3(t+1|t)} & & & \\ R_{2,1}^{-1}\frac{f}{\hat{\mathrm{x}}_3(t+1|t)} & R_{2,2}^{-1}\frac{f}{\hat{\mathrm{x}}_3(t+1|t)} & & & \\ 0 & 0 & & & \\ -(R_{1,1}^{-1}\hat{\mathrm{x}}_1(t+1|t) + R_{1,2}^{-1}\hat{\mathrm{x}}_2(t+1|t))\frac{f}{\hat{\mathrm{x}}_3^2(t+1|t)} & 0 & 0 & 0 \\ -(R_{2,1}^{-1}\hat{\mathrm{x}}_1(t+1|t) + R_{2,2}^{-1}\hat{\mathrm{x}}_2(t+1|t))\frac{f}{\hat{\mathrm{x}}_3^2(t+1|t)} & 0 & 0 & 0 \\ 1 & 0 & 0 & 0 \end{bmatrix} \quad (11)$$

Let $\boldsymbol{H}(t+1)$ denote the extended Kalman filter gain matrix defined by

$$\boldsymbol{H}(t+1) = \boldsymbol{\Sigma}(t+1|t+1)\hat{\boldsymbol{C}}^T(t+1)\,\boldsymbol{\Omega}^{-1}. \quad (12)$$

The extended Kalman filter gain matrix depends on the sensor noise intensity, on the updated covariance matrix and on the inverse rotation matrix $\boldsymbol{R}^{-1}(t)$.

III. Simulation 1, influence of the initial state

We present simulation only for the Extended Kalman Filter (EKF). Very similar results are obtained using the second-order or Gaussian filter [4] (not shown here).

A. Tracker analysis after a 40 Monte Carlo run

The theory of Kalman filtering is based upon the assumption that the noises are Gaussian. In order to trust the statistical significance of stochastic simulations, we run each simulation 40 times. Then we average all the values over the 40 Monte Carlo run. For this simulation we used the following statistics. The diagonal matrices where all the elements but the diagonal ones are equal to zero is denoted by $diag()$, the diagonal elements are expressed between the parenthesis.

Initial true state
$\boldsymbol{x}(t=0) = \boldsymbol{x}_0 = [3.5; -1; -30; 0.1; 0.3; 0]^T$

Mean of the initial state
$\bar{\boldsymbol{x}}(t=0) = \bar{\boldsymbol{x}}_0 = [5; -2; -31; 0.5; 0.2; 0]^T$
Initial state covariance matrix
$\boldsymbol{\Sigma} = \mathrm{diag}\,(2^2; 2^2; 2^2; 0.5^2; 0.5^2; 0.5^2)$

Noise intensity matrices
$\boldsymbol{\Omega} = \mathrm{diag}\,(0.002^2; 0.002^2; 0.5^2)$
$\boldsymbol{\Xi} = \mathrm{diag}\,(0; 0; 0; 0.01^2; 0.01^2; 0.01^2)$

Figure (3) shows the outcome of 40 Monte Carlo runs on the average of the z relative position and velocity as a function of time.

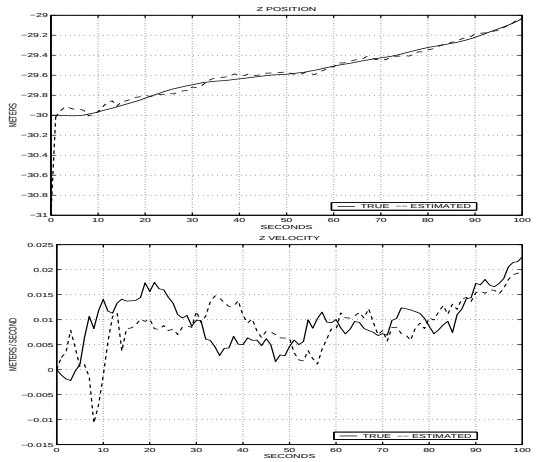

Fig. 3
Average of the relative z position (top)and v_z velocity (bottom)

After a transient period due to the error on the initial true state, the estimated depth converges toward the true one. The relative error in between the true states and the estimates is relatively small; this confirms the good performance of the filter. The increase of relative true and estimated depth is due to the increase of the velocity in the z direction (see Figure 6). As no initial velocity on this direction is applied, the variation of the v_z velocity is due to the plant noise. The computation of the average z velocity over the 40 Monte Carlo runs leads to

$$E\{x_6\} = 0.0098m/s.$$

Hence we can find the variation of the depth

$$\Delta x_3 = E\{x_6\}\Delta t = 0.98m.$$

This result can be verified in Figure 3(top) (At $t = 100s$, $z = -29.04m$). Though the plant noise is not exactly zero mean over an average of 40 simulations, the state estimate on the z position follows closely the true state, and the filter shows good performance. In figure 4, some of the EKF gain elements are plotted. Each element (i, j) corresponds to the correction of the filter on the i^{th} estimated state due to the j^{th} output. Figure 4 demonstrates the strong time-varying nature of some gains.

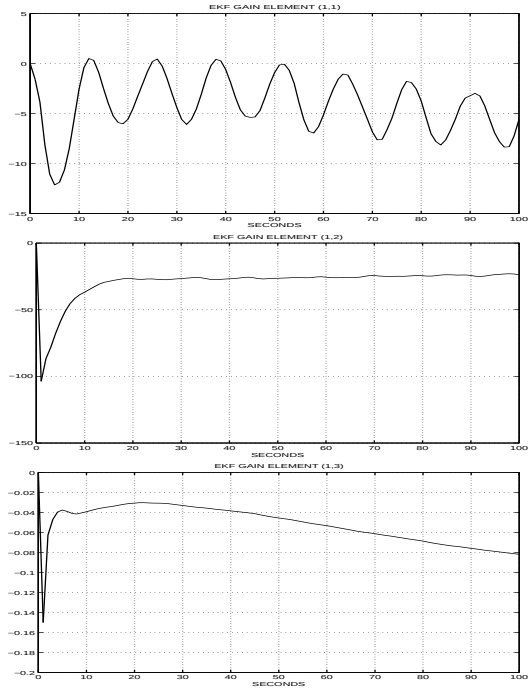

Fig. 4
ELEMENTS (1,1)(TOP), (1,2)(MIDDLE) AND (1,3)(BOTTOM) OF THE EKF GAIN MATRIX

Figures 4 shows that the influence of the measurements $\boldsymbol{z}$ on the x position is mainly due to the y measurement (as explained for Figure 2). As a result, the gain elements $H(1,1)$ is smaller than $H(1,2)$, and the influence of the time varying matrix $\boldsymbol{\lambda}(t)$ can still be seen. The extended Kalman filter resizes the output. The maximum gain peaks on the position 100 (which is the coefficient of the optical magnitude). Hence the influence on x of the third measurement z_3 is less obvious. Similar graphs and reasoning can be obtained for the y position. The EKF gains start with very low values because the dominant terms of the inverse rotation matrix starts from zero (see Figures 2). The peaks, reached during the transient by all the gain elements, are caused by the ratio of the state covariance matrix over the sensor noise covariance matrix as it is shown in (12). Therefore, as the sensor noise intensities are constant, large state covariances lead to high ratio and thus high gain. The extended Kalman filter gains follow the state covariance variations. This simulation illustrates the good performance of our tracker under "good conditions", i.e. small plant and sensor noises as well as small uncertainty on the initial true state. In the next subsection we will see how the tracker behaves if the uncertainty on the initial true state is increased.

B. Influence of the initial state uncertainty

We will now consider three different statistics on the initial true state. The statistics of the plant and sensor noise are kept similar to the previous simulation. The results that follow are averages over 40 Monte Carlo runs.

Initial true state
$\boldsymbol{x}_0 = [3.5; -1; -30; 0.1; 0.3; 0]^T$
Estimate # 1

$\bar{\boldsymbol{x}}_0 = [5; -2; -31; 0.5; 0.2; 0]^T$
$\boldsymbol{\Sigma} = \text{diag}\,(2^2; 2^2; 2^2; 0.5^2; 0.5^2; 0.5^2)$

Estimate # 2
$\bar{\boldsymbol{x}}_0 = [8; -7; -38; 0.5; 0.6; 0]^T$
$\boldsymbol{\Sigma} = \text{diag}\,(10^2; ; 10^2; 10^2; 0.6^2; 0.6^2; 0.6^2)$

Estimate # 3
$\bar{\boldsymbol{x}}_0 = [10; -9; -45; 0.2; 0.8; 0]^T$
$\boldsymbol{\Sigma} = \text{diag}\,(20^2; 20^2; 20^2; 0.7^2; 0.7^2; 0.7^2)$

Figure 5 shows the position and velocity errors for these three cases.
We can observe that once the transient is over, all the estimated states converge toward the true states. The performance of the tracker is satisfying.

IV. SIMULATION 2, CHANGING PLANT NOISE INTENSITY

In this section we compare the performance of our tracker with three different intensities of the plant noise. The results that we obtain are averages over the 40 Monte Carlo runs. In this simulation only the results of the EKF are presented (very similar results are obtained using the second-order or Gaussian filter).

Plant noise intensity # 1
$\boldsymbol{\Xi}_1 = \text{diag}\,(0; 0; 0; 0.01^2; 0.01^2; 0.01^2)$

Plant noise intensity # 2
$\boldsymbol{\Xi}_2 = \text{diag}\,(0; 0; 0; 0.05^2; 0.05^2; 0.02^2)$

Plant noise intensity # 3
$\boldsymbol{\Xi}_3 = \text{diag}\,(0; 0; 0; 0.1^2; 0.1^2; 0.05^2)$

Thus, the standard deviations of the acceleration noise increase for all three variables. Figure 6 shows the updated errors for all the state estimates.
For small relative velocity updated errors, the tracker provides us a good estimation of the position. Though for higher plant noise intensities, the errors on the position increase, the updated errors are acceptable (less than $0.5m$ for the relative position, and less than $0.07m/s$ on the relative velocity). Therefore even for the largest noise intensity, the tracker has good performances, in the sense that maintains both the AUV and ASC near the vertical, as required for hight bandwidth underwater communication .

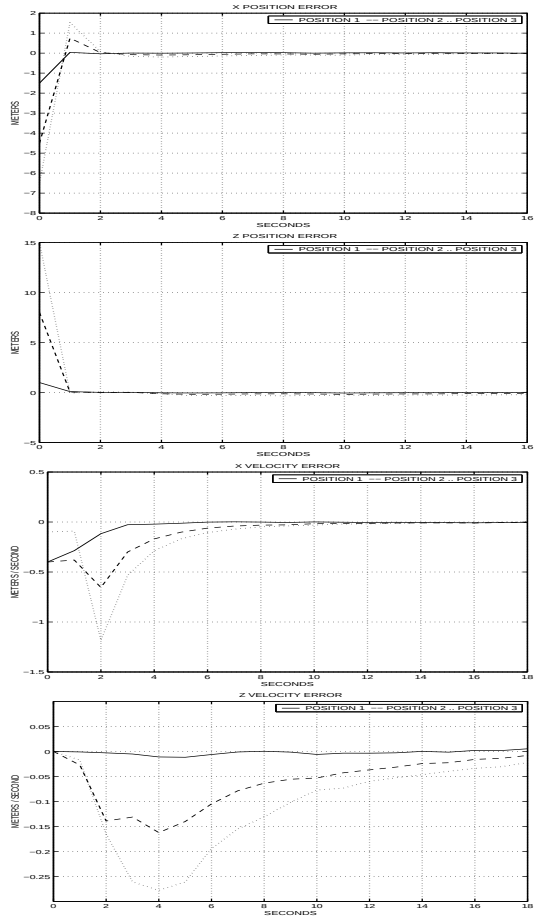

Fig. 5

Relative v_x (top) and v_z (bottom) velocity error

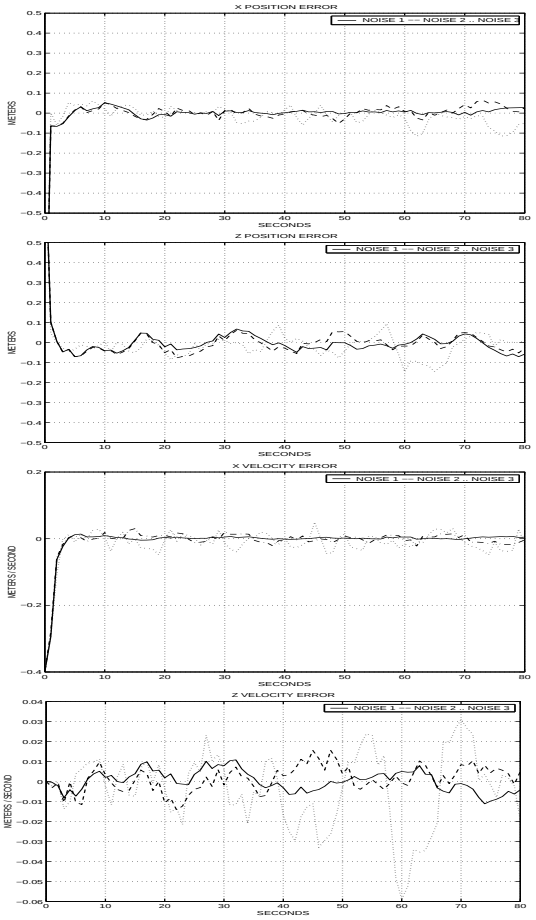

Fig. 6

Updated error for the v_z velocity

V. Conclusion

A non-linear vision-based tracking system was simulated to provide estimates of the position and the velocity of an Autonomous Underwater Vehicle relative to an Autonomous Surface Craft. The system analysis and the design were based on the theory of nonlinear Kalman filtering. Simulations illustrate the good performances of the tracker for different uncertainties on the initial true state and for several intensities of the plant noise. The tracker constructed using the theory of the Second Order Filter (SOF) or Gaussian [4] gives similar results to those obtained with the extended Kalman filter. The additional computations required by the SOF (computation on-line of the Hessian matrices) do not lead to significant accuracy improvements.

The performance of the extended Kalman filter even for a high initial state uncertainty or high plant noise intensity leads to good results. The tracking problem of the platforms is realized in order to minimize the noises on the measurement , and thus to optimize the relative position of the two platforms in order to position them in the vicinity of the vertical position. In this paper we haven't considered any deterministic motion in the plant dynamics. But the goal of this estimator design is to position the two platforms one over the other. Therefore a control loop can be implemented, such as a linear quadratic Gaussian design (LQG), in order to guide the ASC to follow the AUV.

References

[1] ASIMOV (1998-1999), "Advanced Sytem Integration for Managing the Coordinated Operation of Robotic Ocean Vehicles" - ASIMOV. Vol.1-2. Technical Reports. ISR-IST, Lisbon, Portugal.

[2] Balch, T. and R. Arkin, "Communication in reactive multiagent robotic systems," Autonomous Robots 1(1):1-25, 1994.

[3] k P. Oliveira, A. Pascoal, I. Kaminer, " Navigation System Design Using Complementary, Time-Varying Filters," proceeding of 1999 AIAA Guidance, Navigation and Control Conference, Portland Oregon, August 1999.

[4] A. Gelb (ed), "Applied Optimal Estimation," MIT Press, Cambridge, Mass., 1974.